

Reports

Crystal Structure of Benzene II at 25 Kilobars

Abstract. Crystals of a high-pressure form of benzene (benzene II) were grown in the diamond-anvil pressure cell at elevated temperature and pressure from the transition of solid I to solid II. X-ray precession data were obtained from a single-crystal in the high-pressure cell. At 21°C and about 25 kilobars, benzene II crystallizes in the monoclinic system with $a = 5.417 \pm 0.005$ angstroms (S.D.), $b = 5.376 \pm 0.019$ angstroms, $c = 7.532 \pm 0.007$ angstroms, $\beta = 110.00^\circ \pm 0.08^\circ$, space group $P2_1/c$, $\rho_c = 1.26$ grams per cubic centimeter. The crystal structure was solved by generating all possible molecular packing configurations and calculating structure factors, reliability factors, and packing energies for each configuration. This procedure produced a unique solution for the molecular packing of benzene II.

Single-crystal x-ray diffraction techniques at high pressure have been developed in our laboratory during the past few years. The method, described extensively (1-3), uses a beryllium diamond-anvil high-pressure cell and a modified Buerger-type precession camera to obtain x-ray data on single crystals under pressure. It has been demonstrated on a known structure (2) that observed intensity data, after appropriate corrections for absorption, were of such quality that good agreement between observed and calculated structure factors could be obtained.

The first evidence for the existence of a high-pressure modification of benzene, stable at room temperature above 12 kb, was given by Bridgman. He reported the general features of the phase-equilibrium diagram of benzene, and presented *PVT* (pressure, volume, temperature) data on the system up to 50 kb and 200°C (4, 5). In view of the theoretical importance of benzene, an attempt to determine the crystal structure of the high-pressure phase was undertaken.

Extensive study of the phase diagram of benzene (Fig. 1) was carried out visually by a microscopic method which allows observation of the specimen contained in the diamond-anvil cell as the temperature and pressure are varied (6). Liquid benzene readily freezes at ~680 bars at room temperature into a polycrystalline mass (5, 7). A single crystal may be obtained from the mass by reducing the load on the

anvils to allow the crystallites to melt slowly until only one remains in equilibrium with the liquid. If, at this point, the load on the anvils is increased slowly, the crystallite may be made to

Table 1. Crystal data for benzene. The numbers in parentheses are standard deviations on the reported values in units of the last place obtained from least-squares refinement, from 20 experimental values of 2θ .

Benzene I (21°C, ~0.7 kb)	Benzene II (21°C, ~25 kb)
$a = 7.17^*$	$a = 5.417$ (5) Å
$b = 9.28$	$b = 5.376$ (19)
$c = 6.65$	$c = 7.532$ (7)
	$\beta = 110.00$ (8)°
Space group $Pbca$	Space group $P2_1/c$
$Z = 4$	$Z = 2$
$\rho_c = 1.18$ g cm ⁻³	$\rho_c = 1.258$ g cm ⁻³

* For details see (3).

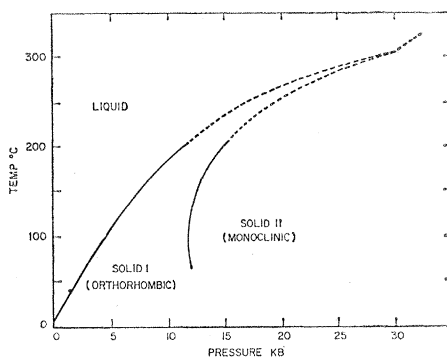


Fig. 1. The equilibrium phase diagram of benzene showing results reported by Bridgman (solid lines) and our results obtained from visual observations and x-ray analysis.

grow. Figure 2 shows a single crystal of benzene I in equilibrium with liquid at ~680 bars and room temperature. The globular appearance of the crystal is characteristic of benzene I near room temperature. At temperatures above 250°C, the crystal loses its globular appearance and begins to assume a crystalline morphology (Fig. 3). By such observations we have extended the phase diagram of this system as indicated by the dashed line in Fig. 1. Although Bridgman proposed that the triple point (liquid-solid I-solid II) should be found at 216°C and 12 kb, our observations indicate that it actually occurs at about 310°C and 30 kb. The transition from I to II is visible at higher temperatures accompanied by increased birefringence of the new phase (II) under polarized light. At room temperature, however, the transition does not take place readily and in some cases cannot be observed until pressures much higher than 12 kb are applied. Figure 4 shows a single crystal of benzene II in equilibrium with liquid at about 310°C and 30 kb. We give estimated pressures in this study because experience with the anvil-type pressure cell has shown that pressures on the specimen cannot be calculated with assurance (8). X-ray precession patterns from a globular crystal showed that the material was well crystallized and that the globular crystal is benzene I (9). The orthorhombic unit cell was found to have the dimensions $a = 7.17$ Å, $b = 9.28$ Å, and $c = 6.65$ Å at 24°C and 700 bars. A more detailed description of benzene I as well as that of five other compounds has been presented (3, 9).

The single crystal of benzene II, from which the x-ray precession intensity data were obtained, was grown from benzene I in the diamond cell at 275°C and 25 kb. This was accomplished by first forming polycrystalline benzene II at pressures above 25 kb. By reducing the force on the anvils, all but one crystallite of phase II were transformed to phase I. The remaining crystallite of phase II was then grown into a large single crystal by transforming the crystallites of phase I into phase II by slowly increasing the load on the anvils. It was possible to follow and check this process by visual microscopic examination. On subsequent cooling to room temperature, the single crystal remained intact in the diamond cell, which was then mounted on the precession camera for analysis. The re-

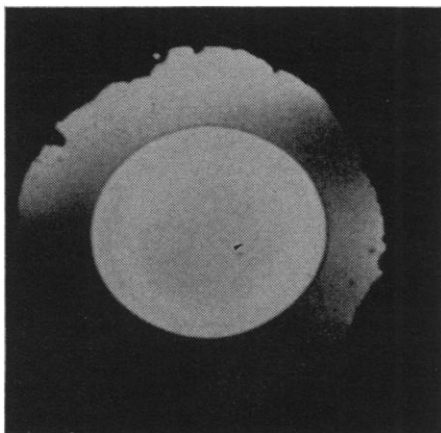


Fig. 2. A globular crystal of benzene I in equilibrium with liquid at 680 bars and room temperature, as viewed through the diamond window of the pressure cell. The irregularly shaped opening is the result of extreme distortion of the metal gasket during the application of pressure and temperature.

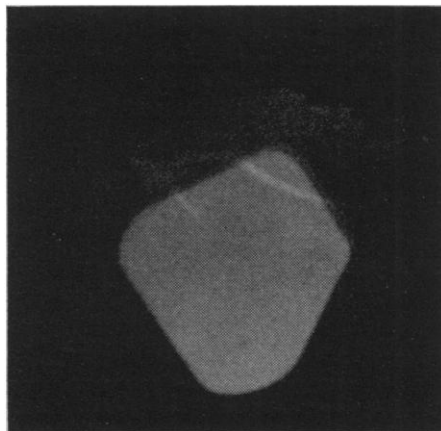


Fig. 3. A crystal of benzene I in equilibrium with liquid at 250°C and about 20 kb, showing the partial formation of faces as viewed through the diamond windows of the pressure cell.

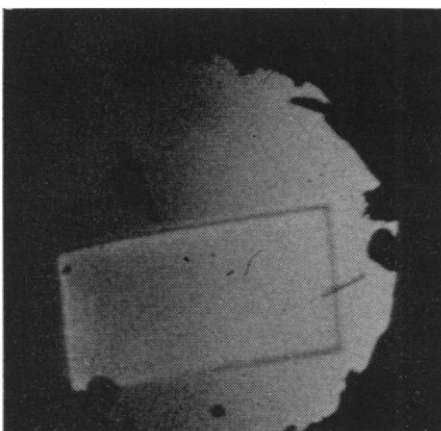


Fig. 4. A crystal of benzene II in equilibrium with liquid at about 310°C and 30 kb, showing well-defined crystal morphology.

sulting x-ray data led to a monoclinic unit cell with $a=5.417$ Å, $b=5.376$ Å, $c=7.532$ Å, and $\beta=110.00^\circ$ at room temperature and 25 kb. By use of these cell dimensions and on the assumption that there are two molecules per cell, the density of benzene II is calculated to be 1.258 g cm $^{-3}$. A comparison of the crystal data for I and II is reported in Table 1.

The x-ray analysis of the crystal of benzene II showed that it was oriented with b^* (where the asterisk refers to the reciprocal parameter) perpendicular to the anvil face and with c^* almost parallel to the dial axis of the precession camera when the long dimension of the pressure cell was vertical. With the crystal in this orientation, certain classes of reflections could not be observed because of the "blind" region arising from the retaining gasket.

For benzene II, five zero-level photographs—including the $h0l$ level—were recorded by precession about the zone axes perpendicular to c^* . In addition, the first upper level along b^* was recorded, which gave $h1l$ data. Because of the specially designed goniometer head, a 70° rotation about b^* could be made which then put a^* parallel to the dial axis. Eight additional zero levels by precession about the zone axes perpendicular to a^* were recorded. With this method of taking data, a number of reflections occur in the photographs of more than one reciprocal lattice plane. By use of these common reflections, the 72 observed intensities were reduced to a single relative scale. Equivalent reflections were averaged to give a set of 19 unique intensities. These are listed in Table 2 along with additional reflections for which the intensity was less than the background. (Because of considerable scattering due to the pressure vessel which the x-rays must penetrate, background levels on the films are high.) For this crystal, no $0k0$ reflections were observed because these reflections occurred in the "blind" region. The $0k0$ reflections were obtained, however, on a second crystal of the material, which grew with c^* perpendicular to the diamond face. The observed extinctions are consistent with the space group $P2_1/c$.

As the space group is $P2_1/c$ with only two molecules per cell, the center of the ring may be placed on the origin. Because there are a limited number of reflections (19 observed), it was decided to generate all possible structures by rotating the ring and to find the struc-

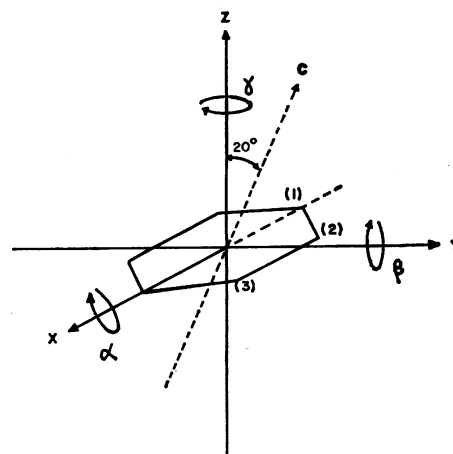


Fig. 5. Initial orientation of the benzene molecule with respect to three mutually perpendicular rotation axes XYZ . The α and β rotation axes are coincident with the a and b parameters of the unit cell, respectively, and the c parameter is 20° away from the rotation axis in the XZ plane.

ture having the best agreement between the observed and calculated structure factors. This procedure is similar to that reported by Damiani *et al.* (10). All subsequent calculations are based on the implicit assumption that, in the pressure range of concern (~ 30 kb), the benzene ring is undistorted (11). Specifically the ring is taken to be a

Table 2. Observed and calculated structure factors. Reflections marked by an "L" were unobserved because their intensity did not exceed the background. They were assigned an intensity slightly less than the smallest observed value. Those marked by an asterisk were measured on a second crystal which was in a different orientation in the cell.

h	k	l	F_{obs}	F_{calc}
1	0	0	26.43	22.55
2	0	0	13.47	14.58
0	0	2	20.53	18.94
1	0	2	12.86	13.54
2	0	2	9.60	13.19
1	0	-2	33.39	33.32
2	0	-2 (L)	5.15	2.62
3	0	-2 (L)	6.98	4.99
0	0	4	6.26	6.73
1	1	0 (L)	3.98	4.20
3	1	0	7.87	8.57
0	1	1	24.37	25.12
1	1	1 (L)	4.98	7.02
2	1	1	10.41	7.54
1	1	-1	16.81	17.05
2	1	-1	11.69	11.29
0	1	2	17.42	18.50
1	1	2 (L)	5.98	1.05
2	1	2 (L)	6.98	2.24
1	1	-2	27.35	27.26
2	1	-2	12.58	11.06
1	1	-3	12.30	12.85
3	1	-3	8.18	8.29
0	1	-4 (L)	6.98	1.42
1	1	-4	11.85	13.60
2	1	-4	11.05	10.43
0	2	0 *	7.35	7.77
0	4	0 *	5.29	5.95

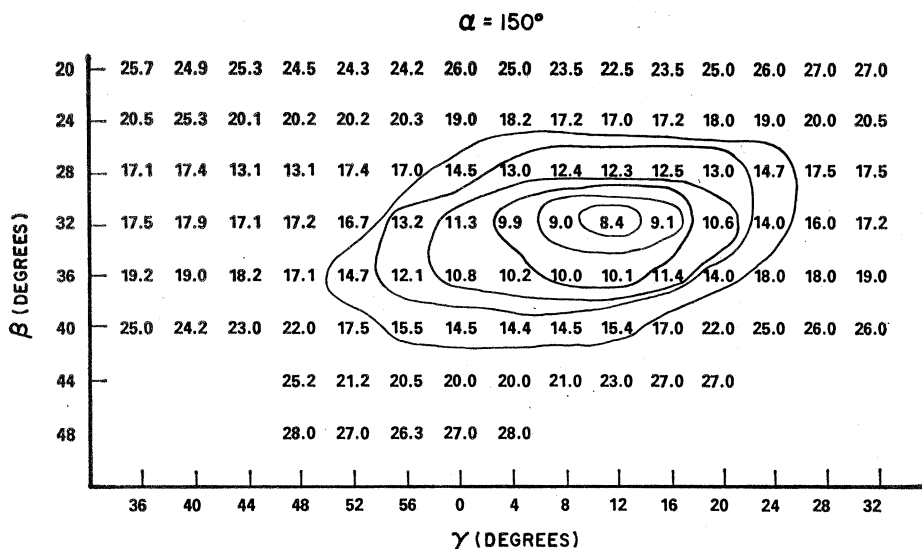


Fig. 6. Average R values as a function of β and γ , at $\alpha = 150^\circ$. For the structure factor calculations, the hydrogen atoms were excluded. No values appear at grid points for values of R greater than 28 percent.

regular planar hexagon, with the C-C bond length being 1.39 Å. A C-H distance of 0.96 Å and 1.08 Å are assumed for structure factor and packing energy calculations, respectively. The short C-H bond distance is consistent with x-ray diffraction studies, and the long distance is consistent with the internuclear separation found in neutron diffraction studies.

The benzene ring is located with its center on the origin of a right-handed orthogonal coordinate system (X, Y, Z). The ring is initially oriented in the XY plane with two of the apices of the ring on the X -axis (Fig. 5). The X -axis and

the Y -axis of this orthogonal coordinate system coincide, respectively, with the a -axis and the b -axis (unique) of the monoclinic cell. The Z -axis makes an angle of 20° with the c -axis of the monoclinic cell. The definition of the structure for the space group $P2_1/c$ requires the coordinates (x, y, z) of three carbon and three hydrogen atoms.

The position of the ring may be altered by α, β, γ rotations about X, Y, Z axes, respectively, and the sense of each rotation is indicated in Fig. 5. For placement of the ring outlined above, a convenient order of rotation is γ first, followed by α , and finally β . Equa-

tions are derived on the assumption of this order, and, if a rotation (α, β, γ) is made, the new coordinates for each atom (x_0, y_0, z_0) are related to the initial coordinates (x, y, z) by the transformation

$$\left. \begin{aligned} x_0 &= -z \cos \alpha \sin \beta + \\ &\quad x(\cos \beta \cos \gamma - \sin \alpha \sin \beta \sin \gamma) \\ &\quad + y(\sin \gamma \cos \beta + \cos \gamma \sin \alpha \sin \beta) \\ y_0 &= z \sin \alpha - x \sin \gamma \cos \alpha + \\ &\quad y \cos \alpha \cos \gamma \\ z_0 &= z \cos \alpha \cos \beta + \\ &\quad x(\sin \gamma \sin \alpha \cos \beta + \cos \gamma \sin \beta) \\ &\quad + y(\sin \beta \sin \gamma - \cos \gamma \sin \alpha \cos \beta) \end{aligned} \right\} (1)$$

The orthogonal coordinates (x_0, y_0, z_0) for each atom are then converted to the monoclinic (m) coordinates in fractions of a unit cell by the equations

$$\left. \begin{aligned} x_m &= (x_0 - z_0 / \tan \beta) / a \\ y_m &= y_0 / b \\ z_m &= (z_0 / \sin \beta) / c \end{aligned} \right\} (2)$$

From the monoclinic coordinates, calculations of structure factors, bond distances, or packing energy may be made for each structure generated by a given rotation (α, β, γ).

Because of the twofold screw axis and the symmetry of the benzene ring, the rotation range for α, β , or γ required to generate all possible configurations is much less than $0-2\pi$. If each rotation angle is allowed a full cycle ($0, 2\pi$) many equivalent and identical configurations are generated. For the structure factor calculations, the ranges should be restricted to the unique range to avoid confusion and to minimize computation time. Gamma is the first rotation, and its unique range is $(0, \pi/3)$ because the ring at (α, β, γ) is identical with a ring at $[\alpha, \beta, (\pi/3) + \gamma]$. Alpha is the second rotation and its unique range is $(\pi/2, \pi)$. Alpha is restricted to the range $(0, \pi)$ as (α, β, γ) is identical to $[\alpha + \pi, \beta, (\pi/3) - \gamma]$, and the range is further restricted to $[(\pi/2), \pi]$ as (α, β, γ) is equivalent to $[(\pi - \alpha), \beta, \gamma]$. Beta is the third and final rotation and its unique range is $(0, \pi)$ as the ring at (α, β, γ) is equivalent to the ring at $[\alpha, (\beta + \pi), \gamma]$.

The ring was rotated throughout the unique range in increments of 4° . The equations used to calculate the structure factors (F_{calc}) are those given in the *International Tables for X-ray Crystallography*, for space group $P2_1/c$ (12). Scattering factors for neutral carbon were taken from the *International Tables for X-ray Crystallography* (13). An isotropic temperature factor (B)

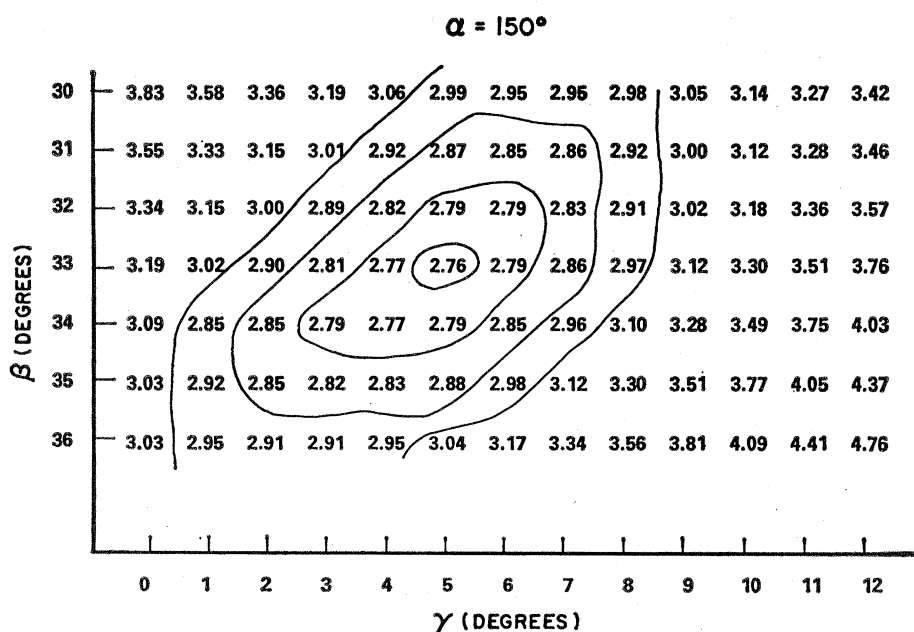


Fig. 7. A plot of relative repulsion energies obtained with Williams' approximation as a function of γ and β at $\alpha = 150^\circ$.

equal to 3.0 was assumed for each of the atoms.

For each orientation a scale factor, $S = \Sigma F_{\text{obs}} / \Sigma F_{\text{calc}}$ and two reliability (R) values were calculated. The first,

$$R_1 = \sum_1^{19} \left| |F_{\text{obs}}| - |F_{\text{calc}}| \right| \left/ \sum_1^{19} F_{\text{obs}} \right.,$$

is the conventional reliability index; and the second,

$$R_2 = \sum_1^{19} \left| \frac{|F_{\text{obs}}| - |F_{\text{calc}}|}{F_{\text{obs}}} \right| \left/ 19 \right.,$$

is an R value which equally weights the reflections. The second reliability index was calculated because the limited amount of data gives the possibility of low R values with some individual agreements being poor, especially for the weaker reflections.

A plot of either type of R value as a function of (α, β, γ) shows that there is only one minimum. Although R_1 and R_2 show minima at the same place, R_2 is much more sensitive as the minimum is much sharper than the minimum in the R_1 plot. Figure 6 shows one section of the plot of R values, and the number plotted at each grid point is the average of R_1 and R_2 . After the approximate position of the minimum was located, subsequent fine scans in 1° rotation increments were made to determine the final structure. This structure has the angular rotations $\alpha = 150 \pm 1^\circ$, $\beta = 33 \pm 1^\circ$, and $\gamma = 6 \pm 1^\circ$ and was calculated by averaging angu-

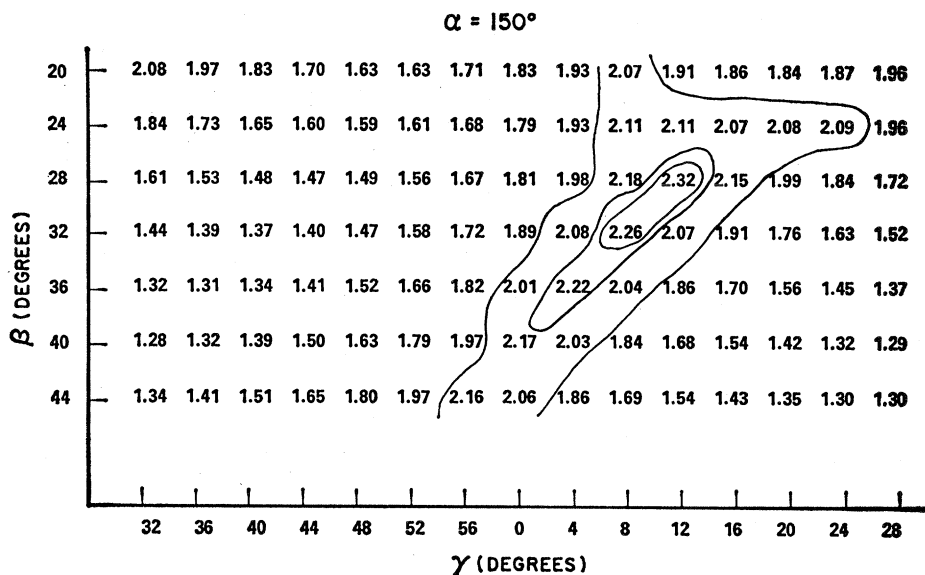


Fig. 8. The minimum closest approach of intermolecular hydrogen interactions is plotted as a function of γ and β at $\alpha = 150^\circ$.

lar settings of the two orientations which gave the minimum R values. The first orientation ($\alpha = 150^\circ$, $\beta = 34^\circ$, $\gamma = 7^\circ$) was obtained from the 19 observed intensities, and the second ($\alpha = 150^\circ$, $\beta = 32^\circ$, $\gamma = 5^\circ$), by including an additional nine reflections whose intensities are less than the minimum observed reflection. The conventional reliability index (R_1) for the final structure is 7.6 percent, and R_2 is 9.1 percent, each based on the 19 observed reflections. The carbon and hydrogen coordinates for this structure are reported in Table 3, and all subsequent calculations of

bond distance with respect to benzene II are based on these parameters. The uncertainties reported for these coordinates are the result of assuming an error of 1 degree for each rotation angle. The observed and calculated structure factors for the final structure are given in Table 2.

In the region bracketing the minimum in R values, the closest intermolecular H...H distances, and an approximation to the packing repulsion energy were calculated. In this region, these calculations were performed at the same values of α, β, γ for which the structure

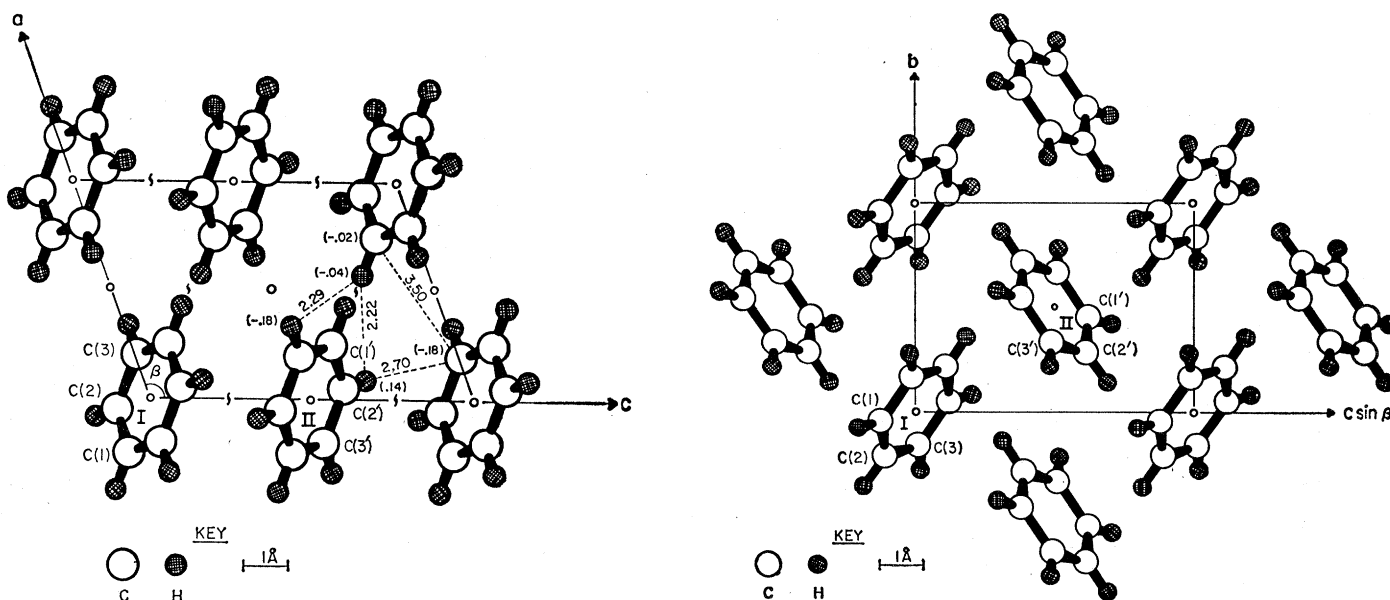


Fig. 9 (left). The projection of the structure of benzene II down the b -axis of the monoclinic cell. The intermolecular distances of closest approach are given for H...H, C...H, and C...C interactions. The y coordinate for the respective atoms is indicated in parentheses. Fig. 10 (right). An orthogonal projection of the structure of benzene II showing the twofold screw axis relationship between rings I and II.

factors were calculated. Plots analogous to the R value plot were made, and one section of each is given in Figs. 7 and 8.

For the energy calculations, the equations

$$\begin{aligned} E_{\text{HH}} &= 1.0(2.88-d_{\text{HH}})^2 & 2.2 \leq d_{\text{HH}} \leq 2.9 \\ E_{\text{CH}} &= 1.56(3.03-d_{\text{CH}})^2 & 2.5 \leq d_{\text{CH}} \leq 3.0 \\ E_{\text{CC}} &= 1.87(3.65-d_{\text{CC}})^2 & 3.2 \leq d_{\text{CC}} \leq 3.6 \end{aligned}$$

as given by Williams (14) were used. At each grid point (representing one α, β, γ setting), the repulsion energy was calculated. This was done by determining all the close intermolecular interactions of the type $\text{C}\cdots\text{C}$, $\text{C}\cdots\text{H}$, and $\text{H}\cdots\text{H}$ where these distances are substituted for d_{CC} , d_{CH} , and d_{HH} in the equations above. The repulsion energy was a minimum at $\alpha=150$, $\beta=33$, $\gamma=5$. The atomic parameters for this orientation are reported in Table 3 along with those found by the structure factor calculation. From Figs. 7 and 8, it is evident that the minimum for the repulsion energy agrees very closely with that for the structure factors and thus provides a confirmation of the structure. The slight difference in minimum in these two plots may be attributable to the assumptions in the C-C and C-H bond lengths used in the calculation of the structure factors and to the constants used in the repulsion energy calculations. Computer programs were written to perform all the types of calculations discussed above—for example, the generation of the settings, the calculation of the structure factors, and the calculation of the packing repulsion energy.

Projections of the structure of benzene II down the b - and a -axes are shown in Figs. 9 and 10, respectively. The closest intermolecular distances of the type $\text{H}\cdots\text{H}$, $\text{C}\cdots\text{H}$, and $\text{C}\cdots\text{C}$ are

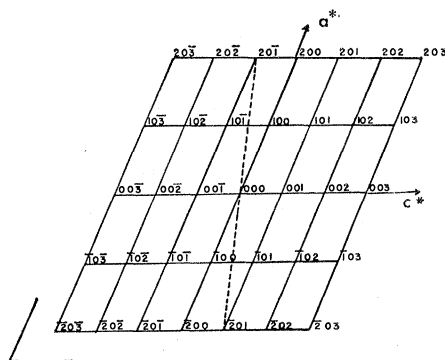


Fig. 11. Diagram of the a^*c^* reciprocal lattice plane of benzene II, showing the mirror twin-plane intersecting the $20\bar{1}$ and 201 and including the b^* axis (dashed line). The angle between this mirror plane and c^* is 90° within experimental error.

indicated in the figures. There are two significant differences between benzene I (9) and II. First, the volume per molecule for benzene II (21°C , 25 kb) is about 23 percent less than for benzene I (-3°C , 1 atm). This volume reduction is consistent with the fact that the closest $\text{H}\cdots\text{H}$ intermolecular distances are 2.23 and 2.64 for benzene II and I, respectively. Second, normals to the planes of two rings related by the screw axis operation in benzene I are nearly orthogonal ($90^\circ 22'$) while the corresponding angle ($\sim 120^\circ$) in benzene II is 30° from orthogonality, which indicates an increased tendency for the planes of the benzene molecules to align themselves more parallel with respect to each other.

Similarities in the structures of benzene I and II permit postulating a mechanism of phase transformation. In this discussion the cell dimensions are referred to as a_m , b_m , c_m (5.42 Å, 5.37 Å, 7.53 Å for monoclinic $\text{C}_6\text{H}_6\text{II}$) and

as a_0 , b_0 , c_0 (7.17 Å, 9.28 Å, 6.65 Å for orthorhombic $\text{C}_6\text{H}_6\text{I}$). The cell dimensions of the orthorhombic phase were measured in the high-pressure cell at about 21°C and 0.7 kb. In the transformation of benzene I to II, discussed below, the cell parameters are related in the following manner: $a_0 \rightarrow c_m$, $b_0 \rightarrow 2a_m$, and $c_0 \rightarrow b_m$.

The arrangement of the molecules in the high-pressure monoclinic phase is pseudo face-centered in the $b_m c_m$ plane. The centers of the rings lie in the $b_m c_m$ plane and are located at each of the four corners and at the center of the face (Fig. 10). Similar packing is present in the low-pressure orthorhombic phase in both the $c_0 a_0$ plane and in the plane parallel to the $c_0 a_0$ plane and intersecting the b -axis at $1/2$. The centers of the rings in this second plane are displaced $\sim 1/2$ cell in c_0 from those in the $c_0 a_0$ plane. In both phases, a twofold screw axis relates the molecules at the center to those at the corners of the pseudo face-centered planes. An important difference between the two phases is the angle of intersection between the normals to the rings related to the screw axes. The ring planes are more nearly parallel in the monoclinic phase.

A possible mechanism of transformation from benzene I to benzene II is a shear between the two planes—the $c_0 a_0$ plane and the plane parallel to the $c_0 a_0$ plane and intersecting the b -axis at $1/2$ —along the c_0 direction. In this shear, the centers of these two planes shift $\sim 1/2 c_0$ relative to each other. After the displacement, the rings readjust to minimize packing energy and the monoclinic high-pressure phase is formed. The value of b_0 (9.28 Å) is effectively halved during this displacement and becomes the monoclinic a_m (5.42 Å). An additional displacement component in the a_0 direction to allow for the β angle in the monoclinic cell is required. A compression along c_0 direction [$6.65 \text{ Å}(c_0) \rightarrow 5.37 \text{ Å}(b_m)$] forces the planes of the molecules less orthogonal to each other. The resulting increased π - π interaction between π -orbitals of adjacent benzene rings then produces increased repulsion in the a_0 direction and may account for the expansion from 7.17 Å(a_0) to 7.53 Å(c_m).

A displacement or martensitic type mechanism for the benzene I to benzene II transition has been suggested on the basis of visual observation of striations produced in the crystal of benzene I on transforming from I \rightarrow II (7).

Table 3. Atomic coordinates for benzene II. The coordinates reported from the structure factor calculation correspond to the angular setting (150° , 33° , 6°) and an assumed C-H distance of 0.95 Å, while those from the repulsion energy calculations correspond to the setting (150° , 33° , 5°) and an assumed C-H distance of 1.08 Å.

Item	x/a	y/b	z/c
<i>Coordinates from structure factor calculations</i>			
C(1)	-0.26140(110)*	-0.02341(200)	-0.11498(180)
C(2)	-0.08015(310)	-0.20459(180)	-0.11875(150)
C(3)	0.18125(200)	-0.18119(20)	-0.00377(340)
H(1)	-0.44006(200)	-0.03940(370)	-0.19357(330)
H(2)	-0.13480(600)	-0.34492(320)	-0.20007(280)
H(3)	0.30525(350)	-0.30552(40)	-0.00650(600)
<i>Coordinates from repulsion energy calculations</i>			
C(1)	-0.26238	-0.01952	-0.11373
C(2)	-0.08460	-0.20297	-0.11985
C(3)	0.17778	-0.18346	-0.00612
H(1)	-0.46624	-0.03468	-0.20210
H(2)	-0.15035	-0.36062	-0.21296
H(3)	0.31589	-0.32594	-0.01086

* The indicated uncertainties in the last place are derived on the basis of an assumed simultaneous error of 1 degree in each of the rotation angles (α, β, γ).

In addition to several crystals grown via the transition of solid I to II, three crystals of benzene II were grown in the diamond cell from the melt at approximately 315°C and ~30 kb. They were cooled to room temperature, and x-ray data were collected on each crystal. Although the cell parameters were identical, each crystal gave data inconsistent with that from the crystal grown from the solid state. Specifically, $h0l$ reflections with l -odd were present—an apparent violation of the extinctions of the space group, $P2_1/c$, assigned to benzene II. Moreover, the diffraction patterns showed an apparent mmm symmetry.

In benzene II, the three reciprocal vectors ending at the nodes—001, 010, $20\bar{1}$ —are perpendicular to each other to within experimental error. These vectors define an end-centered cell with orthorhombic metric symmetry (Fig. 11). These facts can be explained if we assume that benzene II, when grown from the liquid, is twinned by pseudomerohedry. In Fig. 11 the twin mirror plane is indicated by a dashed line, and it contains b^* and the $20\bar{1}$ reflection. With this mirror, the $h0l$ reflections with l -odd can be generated by reflection from the $h0l$ reflections with l -even. Thus the 100 lattice node reflects into the $10\bar{1}$ node. If the two individuals of the twin are present in nearly equal quantities, apparent Laue symmetry mmm would be generated.

Underground Nuclear Explosions and the Control of Earthquakes

Abstract. *Underground nuclear explosions trigger significant earthquake activity for at least 32 hours afterward and to distances up to at least 860 kilometers. The proposed Amchitka test may be used to study the feasibility of employing high-yield underground nuclear explosions to release stresses accumulating in the lithosphere. Periodical explosions along active fault zones may be used to prevent disastrous earthquakes.*

Among the numerous events recognized as trigger mechanisms for earthquakes, only two can be attributed to the activity of man—underground nuclear explosions and the injection of fluids into deep wells (1–3). The association of earthquakes with underground nuclear explosions has been explored in some detail during the past 2 years.

In an examination of records from the University of Nevada's seismographic station network, Boucher *et al.* (2) found that large underground nu-

clear explosions produced a temporary but significant increase in the seismicity of the surrounding region to a degree dependent on the size of the blast. For explosions of magnitudes equal to or greater than 5.0, a substantial increase in activity occurred for at least 1 day following the test. This activity was confined to an area with a radius of about 20 km around the shot point, with a single exception possibly influencing activity to a distance of 40 km. The earthquakes related to nuclear tests were of small magnitude and al-

G. J. PIERMARINI
A. D. MIGHELL
C. E. WEIR, S. BLOCK
*Institute for Materials Research,
National Bureau of Standards,
Washington, D.C. 20234*

References and Notes

1. C. E. Weir, S. Block, G. J. Piermarini, *J. Res. Nat. Bur. Stand.* **69C**, 275 (1965); S. Block, C. E. Weir, G. J. Piermarini, *Science* **148**, 947 (1965); C. E. Weir, G. J. Piermarini, S. Block, *Rev. Sci. Instr.*, in press.
2. A. Santoro, C. E. Weir, S. Block, G. J. Piermarini, *J. Appl. Cryst.* **1**, 101 (1968).
3. C. E. Weir, G. J. Piermarini, S. Block, *J. Chem. Phys.* **50**, 2089 (1969).
4. P. W. Bridgman, *Phys. Rev.* **3**, 153 (1914); *J. Chem. Phys.* **9**, 794 (1941).
5. P. W. Bridgman, *Proc. Amer. Acad. Arts Sci.* **77**, 129 (1949).
6. L. S. Whatley and A. Van Valkenberg, *Advan. High-Pressure Res.* **1**, 327 (1966).
7. R. M. Klein, U. Nourbakhsh, P. N. Adler, *J. Mater. Sci.* **3**, 657 (1968).
8. G. J. Piermarini and C. E. Weir, *J. Res. Nat. Bur. Stand.* **66A**, 325 (1962); *J. Chem. Phys.* **37**, 1887 (1962).
9. E. G. Cox, D. W. J. Cruickshank, J. A. S. Smith, *Proc. Roy. Soc. Ser. A* **247**, 1 (1958).
10. A. Damiani, E. Giglio, A. M. Liquori, *Acta Crystallogr.* **23**, 681 (1967).
11. H. G. Drickamer, *Science* **156**, 1183 (1967).
12. International Union of Crystallography, *International Tables for X-ray Crystallography* (Kynoch Press, Birmingham, England, 1952), vol. 1, p. 383.
13. ———, *ibid.* (1962), vol. 3, p. 202.
14. D. E. Williams, *Science* **159**, 645 (1968).

13 June 1969

Table 1. Total number of earthquakes at 8-hour intervals after each explosion.

Elapsed time (hr)	Earthquakes (No.)
0–8	67
8–16	42
16–24	56
24–32	63
32–40	38
40–48	36
48–56	42
56–64	43
64–72	26
72–80	27
80–88	35
88–96	32
96–104	37

ways at least 1 magnitude unit less than that of the associated explosion. Attempts to ascertain distant effects of these tests indicated that they are probably minor compared with normal variations in seismicity.

Ryall and Savage (3) studied the seismological effects of the 1.2-megaton Boxcar underground nuclear test of 26 April 1968. They recorded thousands of aftershocks within a 6-week period following the explosion, the aftershocks being restricted to an area 12 by 3 to 4 km and to a depth of 12 km. Most of the aftershock hypocenters were found to lie within 5.5 km of the surface, which is shallower than the hypocenters of natural earthquakes in the Nevada region.

We have compared the list of the Nevada underground explosions from 15 September 1961 to 29 September 1966 with a list of earthquakes occurring within 860 km of 37°04'N and 116°15'W, which is roughly at the center of the Nevada test site (4). The explosions and earthquakes within the region and time interval considered totaled 171 and 1109, respectively.

The earthquake list was examined over thirteen 8-hour intervals after each explosion. The expected number of earthquakes in any 8-hour interval, assuming randomness, is 0.2062. The expected number of earthquakes in each 8-hour interval for all explosions, again assuming randomness, is 0.2062×171 or 35.26. The observed numbers for thirteen 8-hour intervals following each explosion are shown in Table 1. Under conditions of randomness, the numbers of Table 1 should be normally distributed around the mean of 35.26 with a standard deviation of $\sqrt{35.26}$ or 5.94. Table 1 shows that this is not the case, the first four numbers averaging almost 4 standard deviations above the mean. It is clear, therefore, that